A numerical-experimental assessment on a composite fuselage barrel vertical drop test: Induced damage onset and evolution

Composite Structures 248 (2020) 112519

Contents lists available at ScienceDirect

Composite Structures

journal homepage: www.elsevier.com/locate/compstruct

A numerical-experimental assessment on a composite fuselage barrel vertical drop test: Induced damage onset and evolution

A. Riccio [a], S. Saputo [a,*], A. Sellitto [a], F. Di Caprio [b], L. Di Palma [b]

[a] Department of Engineering, Università degli studi della Campania "Luigi Vanvitelli", via Roma 29, Aversa (CE), Italy
[b] C.I.R.A Italian Aerospace Research Center, via Maiorise, Capua (CE), Italy

ARTICLE INFO

Keywords:
FEM
Crashworthiness
Fuselage barrel
Composites
Damage evolution

ABSTRACT

Crashworthiness is the ability of a structure to withstand a crash event ensuring the safety of its passengers. The aim of this work is to investigate the damage onset and evolution in a composite fuselage barrel undergoing a vertical drop test on a rigid surface. The mechanical behaviour of the barrel has been assessed by means of a Numerical-Experimental study. Indeed, the experimental data from a full scale barrel test, performed at the CIRA facilities, have been used in conjunction with numerical results, obtained by means of an advanced 3D FEM model, to investigate, in detail, the deformations and the damage development during the crash event. The adopted three-dimensional numerical model, based on an explicit FE formulation, uses Continuum Shell elements and CDM to take into account the onset and the evolution of the intra-laminar damages in each sub-component of the investigated composite fuselage barrel. The obtained numerical results have been compared with experimental data in terms of accelerations, displacements and deformations to provide a preliminary validation of the adopted FEM model. A special attention has been given to sub-components which demonstrated to mainly influence the global mechanical behaviour of the investigated composite fuselage barrel during the experimental test.

1. Introduction

The design of civil aviation structures is conditioned by several constraints related to weight saving, environmental sustainability, costs etc. However, the most important design constraint is the passengers safety, in particular, during catastrophic events such as impact events. Crashworthiness, for an aeronautical structural element, is the ability to withstand an impact by minimising the accelerations transferred to the aircraft cabin [1–4]. Obviously, the level of accelerations transferred to passengers during an impact event is strictly related to the structure's kinetic energy absorption capabilities. The capability to absorb kinetic energy becomes a critical requirement when dealing with carbon fibre reinforced polymers (CFRP) which, nowadays, can be considered the preferred candidates for the manufacturing of aircraft fuselages due to their low specific weight and high specific resistance characteristics. Actually, conventional metallic material aircraft components can absorb most of the impact kinetic energy as plastic deformations, while, CFRPs are characterised by a brittle behaviour without a relevant plastic phase. Hence, for composite materials, crashworthiness capabilities can be achieved by dissipating kinetic energy based on fracture mechanisms such as delaminations, fibre breakage, and matrix cracking [5–12]. The investigation of a composite fuselage impact behaviour is an extremely complex task due to the number of sub-components involved and due to the interactions between the different fracture modes characterising composite structures. Although the full-scale fuselage drop test is the best and direct method to study the effects of an impact on such a complex structure, it is also the most expensive one. Actually, it should be also considered that a number of intermediate tests on sub-components need to be performed in order to correctly interpreter the experimental outputs from the global test in terms of damage onset and propagation. In order to reduce, and correctly perform, these experimental tests, the FAA (Federal Aviation Administration) in collaboration with the NASA (National Aeronautics and Space Administration) have defined an analytical methodology helping in evaluating aircraft design improvements, in terms of crashworthiness, and helping in planning optimised full scale crash tests [13–15]. The layout of sub-components absorbing kinetic energy is related to the

* Corresponding author.
E-mail address: salvatore.saputo@unicampania.it (S. Saputo).

https://doi.org/10.1016/j.compstruct.2020.112519
Received 7 April 2020; Revised 18 May 2020; Accepted 21 May 2020
Available online 26 May 2020
0263-8223/

aircraft size and affects its crashworthiness behaviour. In particular, for medium and large transport civil transportation aircrafts, the sub-cargo floor components have been found to dissipate the most of kinetic energy during an impact without significantly affecting the passenger's cabin [16–21]. Several Authors adopted Finite Element Method (FEM) based numerical models to evaluate the influence of cargo subfloor stiffness, passenger floor stiffness and position, reinforcement of the cabin floor and plastic hinges deformations on the crashworthy behaviour of composite fuselages [22–30]. In order to reduce computational costs, macro-elements simulating complex subcomponents, with suitably calibrated characteristic, have been introduced [30]. More recent works, available in the literature, proposed sandwich structures with composite materials face-sheets for subcargo components, in combination with metallic parts between the frames and the passengers' floor, to improve the energy absorption capabilities [31–33] For each aircraft component, the highly nonlinear geometrical and material behaviour has been taken into account to correctly investigate the global mechanical behaviour during the impact event [34–38]. The definition of an optimal design of a complex composite structure is strongly influenced by the strength characteristics of the material, especially when the absorption of kinetic energy by failure mechanisms is of primary concern. Actually, the dissipation of kinetic energy by damages can occur according to several failure mechanisms, mainly intralaminar failure mechanisms such as fibre and matrix breakage in traction and/or compression. These damages arise during the impact phenomenon and evolve leading to the structural collapse. For this reason, the theories for predicting the damage onset and evolution, which are useful for understanding and describing the complex interacting failure mechanisms in composite materials are of great interest, especially during crash events. In the literature, several fracture mechanics theories, able to accurately describe the failure mechanisms arising and evolving in aeronautical composite structures, can be found [39–48].

Indeed, the continuous damage mechanics (CDM) theory is mainly adopted for the evaluation of the intralaminar damages in composite aircraft components. According to this theory, the reduction of the stiffness of the structure can be physically associated to the presence of distributed micro-fractures or defects. In the present work the onset and the evolution of damages in a composite fuselage barrel undergoing a drop test on a rigid ground at a pitch angle of about 2.28°, have been assessed. The considered fuselage barrel is an assembly of subcomponents made of different materials: woven carbon plies have been adopted for the cargo area and the passenger's floor, unidirectional long fibre carbon plies have been used for the manufacturing of the stringers, frames and skins and an aluminium alloy has been adopted for the hinges and the struts. Data from the experimental drop test on the full-scale fuselage barrel [49] have been used in conjunction with an advanced Finite Element Method based model to investigate the influence of the damage development within sub-components on the global fuselage barrel impact behaviour. The finite element model has been developed within the Abaqus/Explicit environment with continuum shell elements. The stiffness of the composite material has been degraded at lamina level by means of damage coefficients as stated by Hashin's failure criteria, while, for the aluminium alloy, a failure criterion for ductile metallic materials has been adopted. The results obtained from the numerical model have been compared to experimental data in terms of deformations, vertical displacements, and acceleration to study in detail the failure mechanisms arising, evolving and interacting during the impact event. The experimental drop test reported in [49] has been briefly described here in Section 2. Then, a brief theoretical background on the damage models, adopted to take into account intra-laminar damage onset and propagation, has been introduced in Section 3 together with the barrel geometrical and FEM model descriptions. Finally, in Section 4, the numerical results have been presented and compared to experimental data in terms of deformations, vertical displacements, accelerations and damage development in sub-components, which demonstrated to mainly influence the global mechanical behaviour of the investigated composite fuselage barrel during the experimental test.

2. Experimental drop test

In this section, details on the drop test performed on the fuselage section analysed in the present paper have been given. Information on the fuselage boundary conditions during the test preparation and during the test execution [49], useful for the definition of the numerical model, have been provided. The drop test of the fuselage section has been carried out with the aid of a crane to reach the height required to perform the test. In particular, the release system between the fuselage and the crane hook is shown in Fig. 1.

The connection between the crane hook and the fuselage section has been achieved by using four bands suitably linked to the four central windows (two for each side) by means of metal handles, as shown in Fig. 2.

The windows and handles closure system installed to perform the drop test are shown in Fig. 2. The mass of the whole support system adopted for the test is approximately 23 kg.

Indeed, a total weight of 957 kg for the fuselage section has been verified before the installation of interiors, test instrumentation, handles etc. The additional masses, added by the plugs and handles installed in the windows, the data acquisition system, the dummies and the seats, have been considered in the frame of the performed numerical computations.

In order to assess the acceleration transferred to occupants as a consequence of the fuselage impact, useful to investigate the mechanical response in terms of crashworthiness of the adopted fuselage section, two dummies, respectively Hybrid II and FAA Hybrid III, have been installed in the forward part of the fuselage. The dummies have been positioned on aeronautical seats installed along the first window row, between the third and the fourth frames. Indeed, a seats set, as shown in Fig. 3, composed by three seats and four cabin floor hooks, characterised by a total mass of about 185 kg, has been installed.

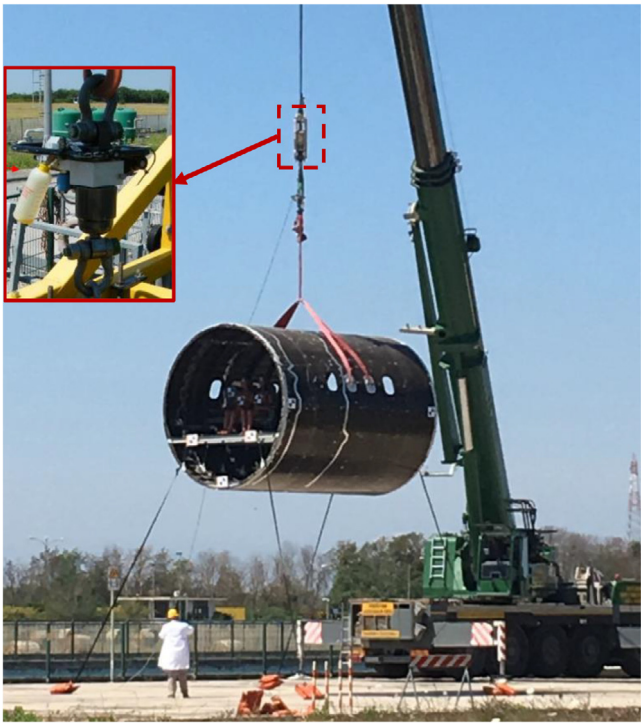

Fig. 1. Drop test release system.

Fig. 2. A) Bands used to raise the section fuselage; B) Metal plug with handle.

The test article has been also equipped with a data acquisition system including a damping mass to avoid accelerations able to invalidating the measured data. Also masses balancing the weight of the seats and dummies have been incorporated in the test article. During the drop test, due to the unbalancing effect generated by gusts of wind, the fuselage barrel experienced small roll and pitch rotations just before touching the ground. Markers have been placed on the fuselage barrel in order to experimentally evaluate the displacements at specific locations by means of high speed cameras. The first two locations, well-defined by the markers positioned on the first crossbar of the passengers' floor, in the middle of the fixing rails of the passenger seats and in the front part of the fuselage barrel, have been named as Marker A1 and A2 (see Fig. 4-A). While, the remaining two locations, named as Marker B1 and B2, are positioned at the edges of the fuselage barrel along the middle longitudinal axis of the aircraft, as shown in Fig. 4-B.

Fig. 5 A-B shows the roll and pitch angles measured at impact with the ground. These angles have been evaluated by measuring the distances between markers positioned, respectively, on the forward passenger's floor support and on the lateral skin, according to images from a high-speed camera. These angles have considered during numerical computations in order to correctly compute the stress distribution and the damage evolution in the fuselage barrel sub-components.

3. Theoretical background and numerical model description

As already mentioned, the experimental activity performed on the investigated fuselage barrel has allowed to identify the damage status at the end of the impact test and to evaluate the acceleration transferred to the occupants. However, in order to assess the full mechanical response of the fuselage barrel during the crash event, including the damage onset, damage evolution and the stress redistribution in each sub-component leading to the experimentally verified final acceleration and damage status experienced by the barrel, an extensive numerical activity has been carried out. Indeed, the adoption of an advanced numerical model has allowed to identify drivers in crashworthy design, for identified key sub-components, able to significantly influence the barrel global mechanical behaviour during the crash event. In this paragraph, details on the theoretical background, in terms of composites damage evolution methodologies, implemented in the numerical model adopted for the computations, are firstly introduced; then, geometry, materials, and boundary conditions applied to the Finite Element model, adopted to simulate the experimental drop test, are showed.

3.1. Theoretical background

In the frame of the proposed numerical model, intra-laminar damage has been considered to evaluate the degradation of composite sub-components during the crash event. Indeed, Hashin's failure criteria [50] together with material gradual degradation rules [50] have been applied to evaluate the intra-laminar damage on-set and propagation in terms of fibre and matrix breakage in composite sub-components. On the other hand, a standard bilinear ductile metallic criteria have been used to predict the damage on-set and evolution for metallic parts. The polynomial Hashin's failure criteria, allowing to detect the damage onset of matrix and fibre under traction and compression loading conditions, are introduced as Eqs. (1)–(4):

Fibre in tension

$$F_{ft} = \left(\frac{\widehat{\sigma}_{11}}{X_T}\right)^2 + \alpha\left(\frac{\widehat{\sigma}_{12}}{S_L}\right)^2 = 1 \tag{1}$$

Fibre in compression

$$F_{fc} = \left(\frac{\widehat{\sigma}_{11}}{X_C}\right)^2 = 1 \tag{2}$$

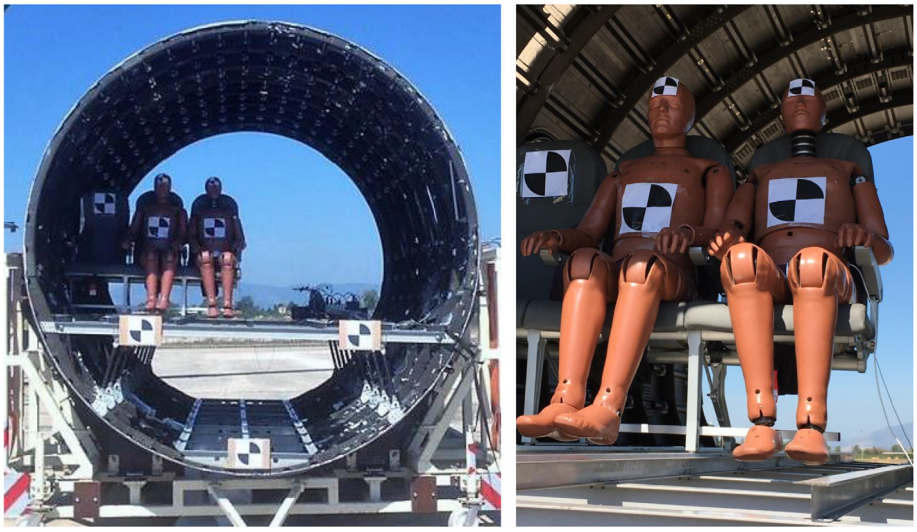

Fig. 3. Dummies and seats.

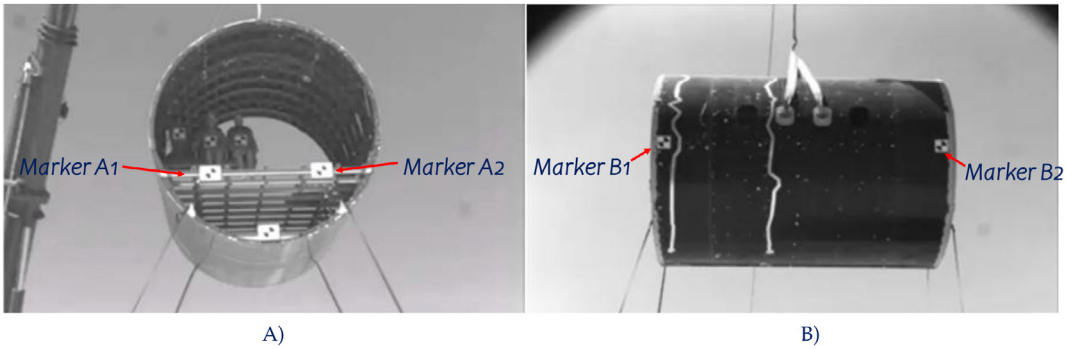

Fig. 4. Marker displacement positions. A) Frontal view. B) Lateral view.

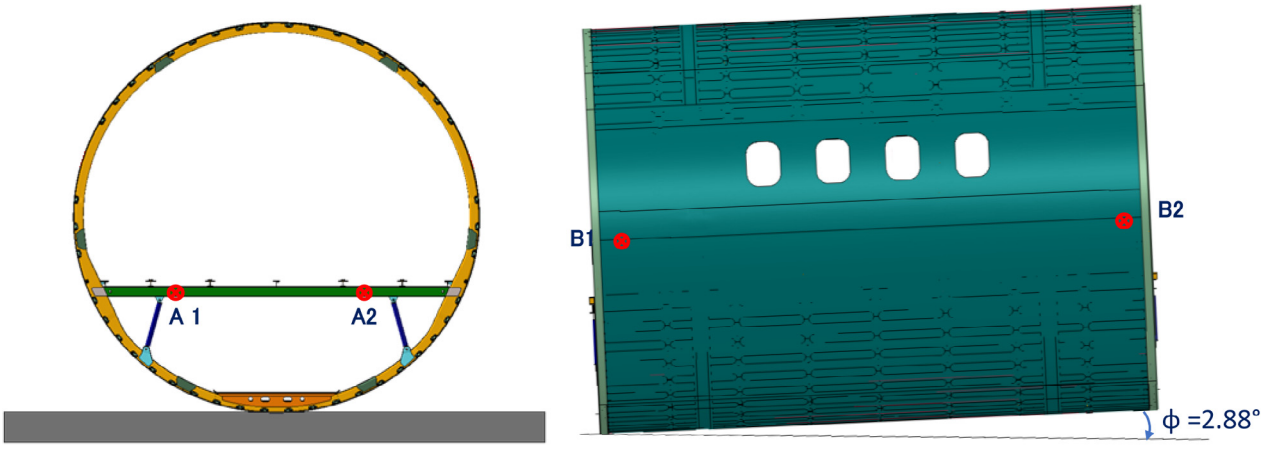

Fig. 5. Pitch an roll angles measured during the drop test (at impact with the ground).

Matrix in tension

$$F_{mt} = \left(\frac{\widehat{\sigma}_{22}}{Y_T}\right)^2 + \left(\frac{\widehat{\sigma}_{12}}{S_L}\right)^2 = 1 \tag{3}$$

Matrix in compression

$$F_{mc} = \left(\frac{\widehat{\sigma}_{22}}{2S_T}\right)^2 + \left[\left(\frac{Y_C}{2S_T}\right)^2 - 1\right]\cdot\frac{\widehat{\sigma}_{22}}{Y_C} + \left(\frac{\widehat{\sigma}_{12}}{S_L}\right)^2 = 1 \tag{4}$$

where $\widehat{\sigma}_{11}$,$\widehat{\sigma}_{22}$,$\widehat{\sigma}_{12}$ are the effective stress components evaluated along the fibres direction, matrix direction and shear. XT, XC, YT, YC, SL, and ST are, respectively, the fibre tensile and compression, matrix tensile and compression, and shear strength in longitudinal and transverse directions. α is a coefficient that determines the contribution of the shear stress to the fibre tensile initiation criterion, for this specific application a constant value of α = 1 has been used. Fig. 7 shows the degradation rule adopted to simulate the damage onset and evolution phases for each failure mode at lamina level in each Finite Element.

According to Fig. 6, at point A the Hashin's failure criteria are satisfied resulting in a damage onset "status". Then, the damage evolution phase takes gradually place along the segment AB, up to the maximum equivalent displacement t δ^f_{eq} where the lamina can be considered fully damaged [51]. The damage evolution phase takes place by linearly degrading the elastic properties at lamina level, according to a stiffness material degradation coefficient *d*. The four different degradation coefficients adopted in the frame of the numerical simulations, one for each failure mode, are introduced in Equation (5).

$$d_i = \frac{\delta^f_{i,eq}\left(\delta_{i,eq} - \delta^0_{i,eq}\right)}{\delta_{i,eq}\left(\delta^f_{i,eq} - \delta^0_{i,eq}\right)}; \quad \delta^0_{i,eq} \le \delta_{i,eq} \le \delta^f_{i,eq}; \quad i \in (f_c, f_t, m_c, m_t) \tag{5}$$

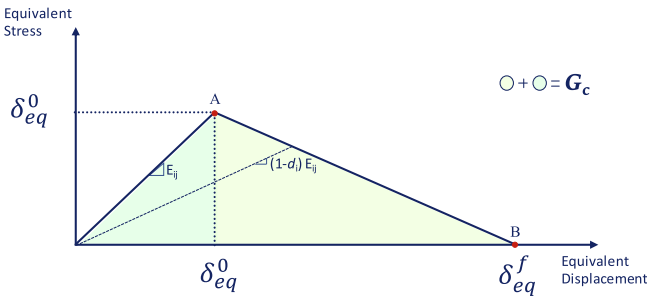

Fig. 6. Constitutive relation (damage evolution).

The maximum equivalent displacement is evaluated according to Equation (6).

$$\delta^f_{i,eq} = \frac{2G_{ic}}{\sigma^0_{i,eq}}; i \in (f_c, f_t, m_c, m_t); \tag{6}$$

$\sigma^0_{i,eq}, \delta^0_{i,eq}$ are respectively the equivalent stress and displacement at the Hashin's failure criteria limit conditions (Point A in Fig. 6). Gic is the material fracture toughness related to fibre and matrix, compression and tensile failure modes. In Table 1, the relations adopted to evaluate the equivalent stresses and displacements are introduced.

L_c is the characteristic length, introduced to mitigate the mesh dependence issue, and < > represents the Macauley bracket operator [51].

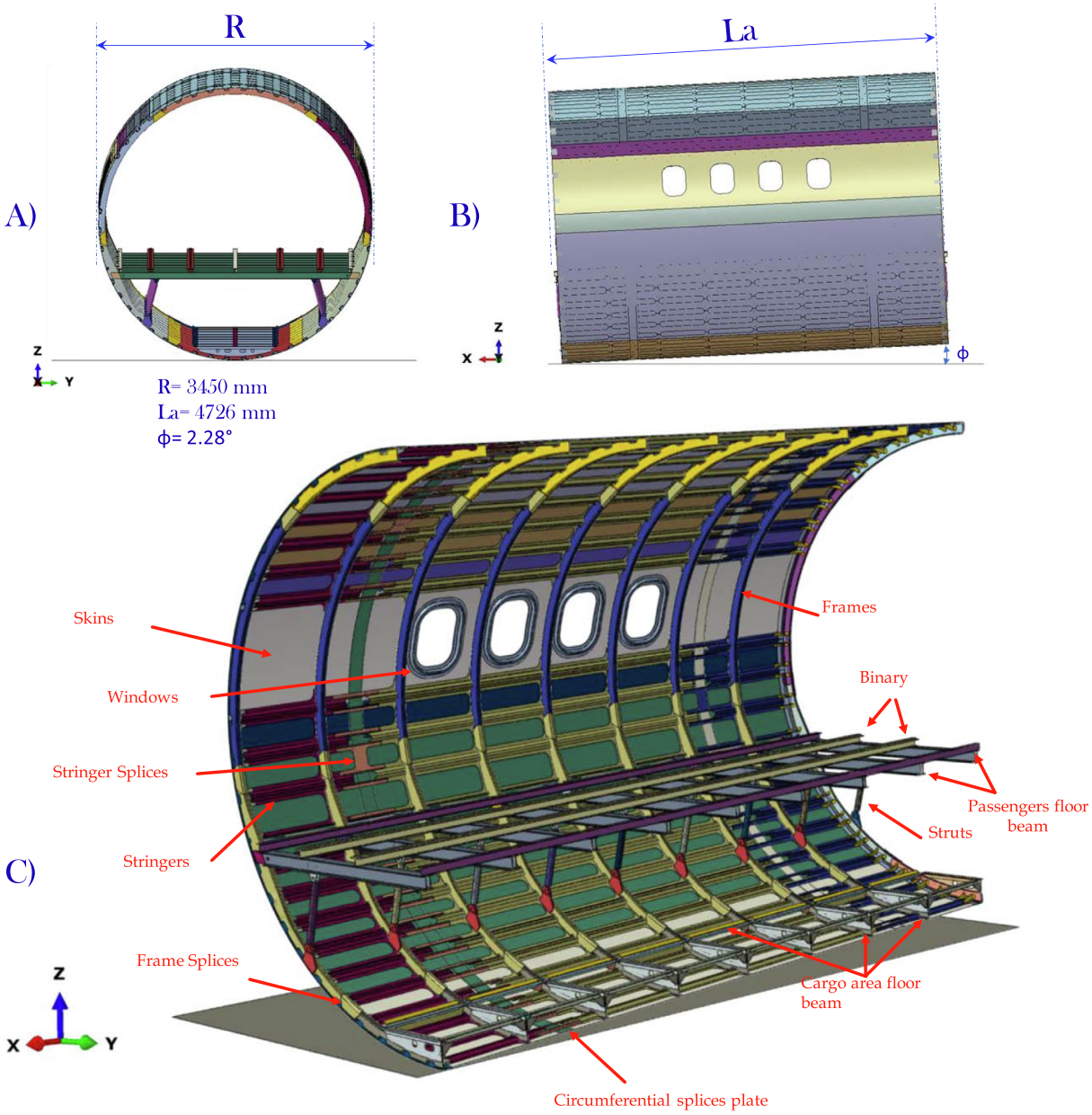

Fig. 7. Geometrical fuselage barrel description. A: Frontal view. B: Lateral view. C: Section Isometric view.

Table 1
Equivalent stresses and displacements definition.

	Equivalent Stress	Equivalent Displacement
Fibre Tension	$\frac{L_c(\langle\sigma_{11}\rangle\langle\varepsilon_{11}\rangle+\sigma_{12}\cdot\varepsilon_{12})}{\delta_{ft,eq}}$	$L_c\sqrt{\langle\varepsilon_{11}\rangle^2+\varepsilon_{12}^2}$
Fibre Compression	$\frac{L_c-\langle\sigma_{11}\rangle-\langle\varepsilon_{11}\rangle}{\delta_{fc,eq}}$	$L_c\langle-\varepsilon_{11}\rangle$
Matrix tension	$\frac{L_c(\langle\sigma_{22}\rangle,+\langle\sigma_{12}\rangle\cdot\varepsilon_{12})}{\delta_{mt,eq}}$	$L_c\sqrt{\langle\varepsilon_{22}\rangle^2+\varepsilon_{12}^2}$
Matrix Compression	$\frac{L_c(\langle-\sigma_{22}\rangle-\langle\varepsilon_{22}\rangle+\sigma_{12}\cdot\varepsilon_{12})}{\delta_{mc,eq}}$	$L_c\sqrt{\langle-\varepsilon_{22}\rangle^2+\varepsilon_{12}^2}$

3.2. Geometrical description of the investigated test article

The geometrical description of the investigated fuselage barrel are introduced in Fig. 7 where sub-components (skin, frames, stringers, stinger splices, passengers floor beams, Cargo floor beam, binary, windows, circumferential splice plate, struts) have been represented with different colors. As it can appreciated in Fig. 7-B, the pitch angle of impact between the fuselage section and the ground (2.28°) measured during the test, has been taken into account in the frame of the numerical simulations. Finally, in Fig. 7-C an isometric view of the section fuselage is provided.

3.3. Materials description

Three different material systems have been adopted to manufacture the investigated fuselage barrel: a unidirectional long-fibre composite material system, a woven fabric composite material system and the Al2025 aluminium alloy. According to Fig. 8, it is possible to identify the material composition of each sub-component.

In Table 2 and Table 3, the mechanical properties adopted for the numerical simulations are introduced. Indeed, in Table 2, the material properties of the unidirectional and the woven fabric composite material systems are detailed while in Table 3, the material properties of the adopted aluminium alloy are shown.

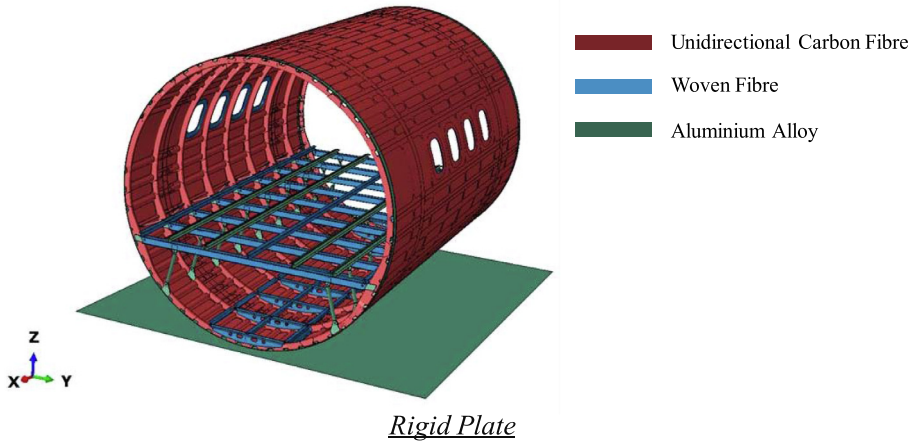

Fig. 8. Material description for fuselage section.

Table 2
Composite materials properties.

	Composite materials			
Young's Modulus, E_{11} [MPa]	Fibre composite material	137,500	Woven fabric material	55,000
Young's Modulus, E_{22} [MPa]		8200		55,000
Shear Modulus G_{12} [MPa]		3950		3363
Shear Modulus G_{13} [MPa]		3950		3363
Shear Modulus G_{23} [MPa]		3950		3363
Poisson's ratio $\nu_{12} = \nu_{13} = \nu_{23}$		0.35		0.30
Fibre Tensile Strength F_{1t} [MPa]		1890		650
Fibre Compressive Strength F_{1c} [MPa]		1008		650
Matrix Tensile Strength F_{2t} [MPa]		86.5		650
Matrix Compressive Strength F_{2c} [MPa]		112		650
In-Plane Shear Strength, S_{12} [MPa]		95		150
Out-Plane Shear Strength, S_{23} [MPa]		100		150
Fracture toughness energy fibre tensile [kJ/m^2]		130		58
Fracture toughness energy fibre compression [kJ/m^2]		102		58
Fracture toughness energy fibre in traction [kJ/m^2]		46		58
Fracture toughness energy fibre in traction [kJ/m^2]		83		58
Density [ton/mm^3]		1.9 e^{-9}		1.97 e^{-9}
Ply thickness [mm]		0.129		0.25

Table 3
Aluminium alloy mechanical properties.

Aluminium Al2025	
Young's Modulus, E [MPa]	70,000
Poisson's ratio ν	0.33
Yield stress [MPa]	369
Ultimate Tensile stress [MPa]	469
Density [ton/mm^3]	2.7 e^{-9}

Table 4
Composite component parts stacking sequence.

Stacking Sequence	
Skin	$[90/45/0/45]_s$
Stringer	$[45/45/0/0/90/0/0]_s$
frames	$[90/45/0/45/-45/90/45/45/0-45/45-45]_s$
Components in Woven fabric material	$[0/45/0-45]_s$

The stacking sequences adopted for the different sub-components constituting the fuselage barrel are introduced in Table 4. For aluminium alloy made subcomponents a thickness of 8 mm has been used. Furthermore, a damage criterion based on Continuum Damage Mechanics (CDM) has been adopted for the aluminium parts. A ductile criterion [52] has been used for the determination of the equivalent plastic strain at damage initiation, while a damage evolution law based on the evaluation of a scalar damage variable has been adopted for the simulation of the damage progression up to final failure.

3.4. Finite element model description

A Finite Element Model of the investigated fuselage barrel with 2,027,708 nodes and 102,151 elements has been defined in the ABAQUS Explicit FEM environment. Both the unidirectional and woven fabric composite components have been modelled by using 8-noded continuum shell elements with a reduced integration scheme. For the aluminium components, elements with a solid formulation, with 8 nodes and a reduced integration scheme, have been used. For the stanchions, also made of aluminium, a three-dimensional discretization has been chosen for the central body, while the connection bolts between the stanchions and the surrounding structure have been modelled by Abaqus connector elements able to transfer all the degrees of freedom between the sub-components. The failure criteria adopted for the stanchion are the same used for the other aluminium components: continuum mechanics based plastic initiation-evolution law for ductile materials. The fuselage sub-components have been connected each

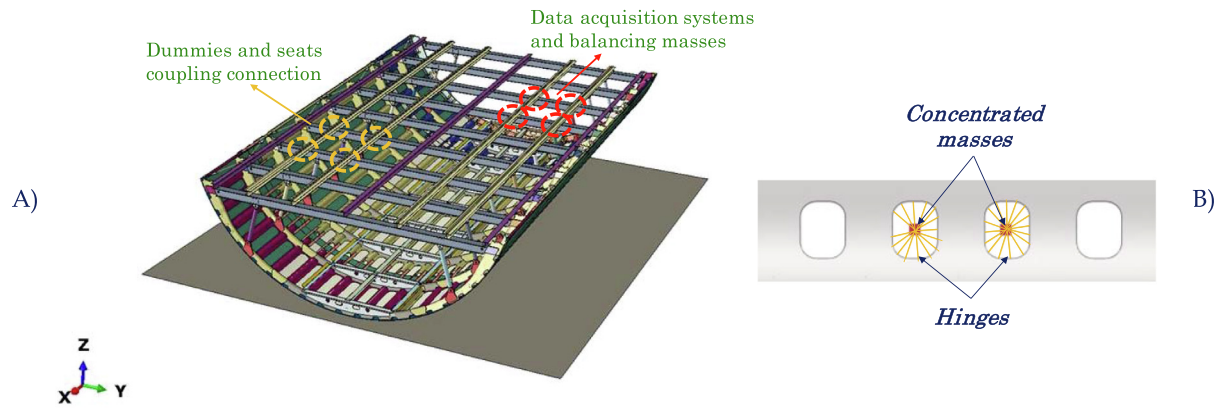

Fig. 9. Concentrated masses position: A) Dummies, seats and data acquisition system masses. B) Windows and hinges masses.

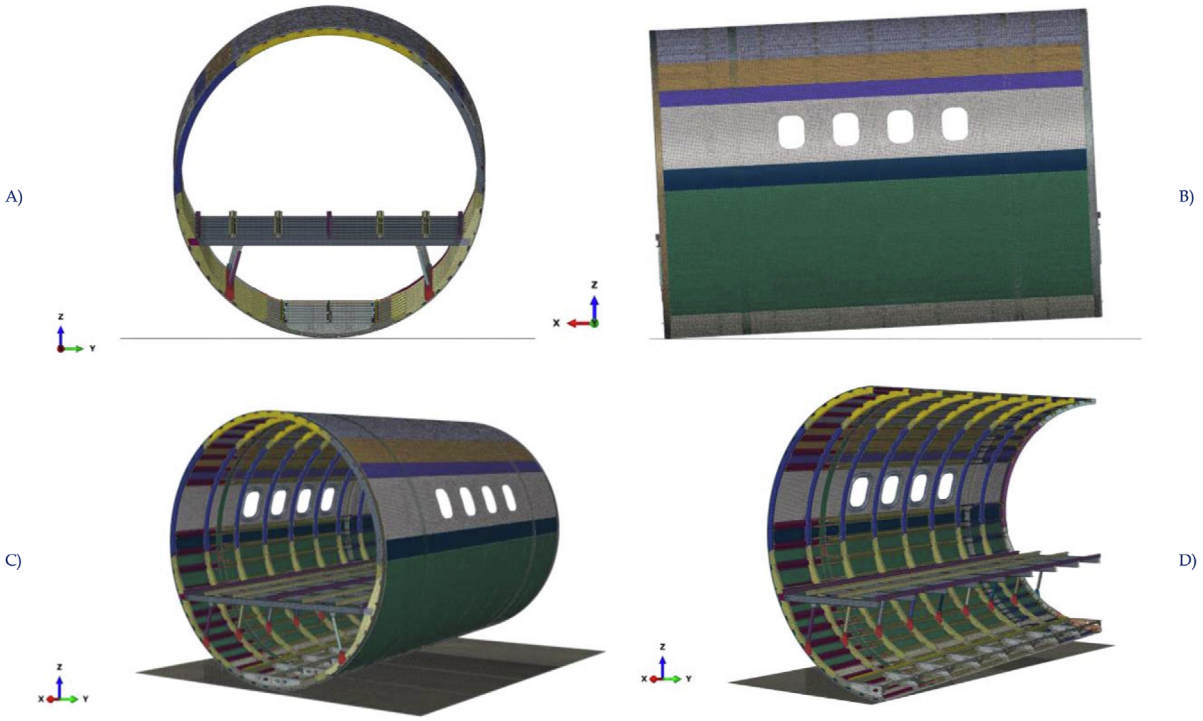

Fig. 10. Discretized fuselage barrel: A) Frontal view. B) Lateral view. C) Isometric view. D) Fuselage section isometric view.

other by means of tie constraints avoiding mesh coincidence at interfaces [51]. Actually, the neglection of rivets holes clearance and deformations can induce local stiffening effects.

In order to provide a realistic prediction of the mechanical response of the considered fuselage section during the drop test, point masses have been introduced to take into account the additional non-structural masses added to the fuselage barrel before the drop test (instruments, setas, dummies, handels etc). Moreover, the windows handles, used for connection to the crane hook, have been replaced with kinematic couplings between the windows edges and the windows centre point where a concentrated mass, representative of the entire handles, has been applied. Fig. 9 shows the positions, on the fuselage barrel passenger's floor, of the seats' connections, the data acquisition system and the masses balancing seats and dummies.

The concentrated masses, representative of the instrumentations, have been positioned 45 mm higher with respect to the passengers' floor; while the masses representing the seats, the dummies and the balancing masses have been positioned at an height of 500 mm from the passengers' floor.

In Fig. 10A-B-C, the front, the lateral and the isometric views of the discretized fuselage barrel are presented; while in Fig. 10- D, details of the Finite Elements discretization adopted for the fuselage subcomponents are given. In order to numerically evaluate the acceleration at key locations of the fuselage, accelerometer elements have been introduced in the Finite Element Model. The locations of the accelerometer elements are highlighted in Fig. 11. Actually, the following accelerometer elements have been positioned in the middle section of the barrel model corresponding to accelerometers position in the real fuselage barrel subjected to the drop test:

- Accelerometer element I to evaluated the acceleration of the cargo area;
- Accelerometer element II to evaluated the acceleration on the passenger floor;
- Accelerometer element III on the upper part of the fuselage.

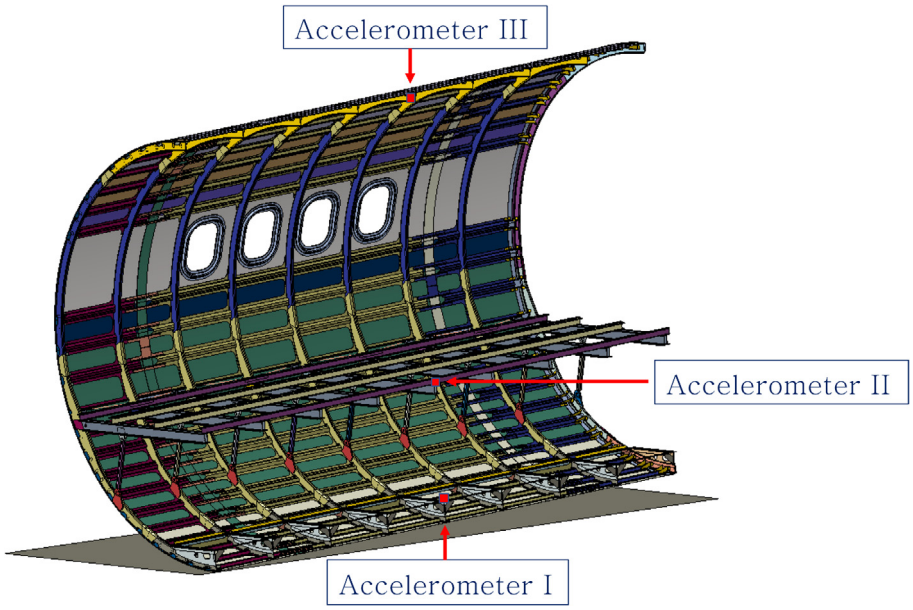

Fig. 11. Accelerometer elements' position.

As mentioned in the previous section, due to external conditions (wind), the fuselage barrel touched the ground, during the drop test, with non-zero pitch and roll angles. In the frame of the numerical simulations, the fuselage barrel has been positioned with a 2.28° pitch angle with respect to the ground to allow the realistic prediction of its mechanical response. On the other hand, the roll angle has been neglected since its influence on the mechanical response of the fuselage barrel has been considered not significant. The impact with the ground has been simulated by introducing a rigid plate 5.5 × 4.5 m^2-wide and by setting an initial velocity of 9.14 m/s in the z-direction to all the nodes of the fuselage barrel.

4. Results and discussion

In this section, experimental data from the drop test performed at the CIRA (Italian Aerospace Research Centre) LISA (Laboratory for Impact of Aerospace Structures) plant [50] have been analysed with the aid of the numerical results obtained with the FE model proposed in the frame of the present paper, in order to fully understand the mechanical response of the investigated fuselage barrel in terms of displacements, deformations, accelerations and damage development. Indeed, a first validation of the introduced numerical model has been carried out by comparing experimental and numerical results in terms of displacements, acceleration and deformed shapes. Then, the numerical results in terms of damage onset and evolution during the impact event have been adopted to identify the key sub-components which mostly influence the energy absorbing capability of the fuselage barrel.

A first comparison between the experimentally and numerically determined vertical displacements, during the impact event up to the maximum vertical displacement, at the four locations identified in Fig. 6, has been carried out. Indeed, in order to optimise the computational effort, the simulation of the drop test has been performed by positioning the fuselage barrel at 1 mm from the target rigid surface and setting on all nodes an initial speed without taking into account the gravitational field. In these conditions, only the numerically simulated mechanical response up to the maximum vertical displacement can be considered reliable since, without the presence of the gravitational field, the fuselage finite element model, differently from the real fuselage, is able to invert its motion. This approximation in numerical analyses has been considered acceptable since the most of the damage onset and evolution phenomena take place from the beginning of the impact event up to the time the maximum vertical displacement is reached.

In Fig. 12-A the experimental and numerical vertical displacements of marker A1 and A2 (frontal displacements, see Fig. 5-A) are compared. A similar comparison for the marker B1 and B2 (lateral displacements, see Fig. 5-B) are introduced in Fig. 12-B. This first comparison in terms of vertical displacements show an excellent agreement between the experimental data and the numerical results up to the point of maximum vertical displacement. Actually, the numerical and the experimental curves are almost overlapped. The excellent agreement between the slopes of the numerical and experimental curves demonstrates the capability of the numerical model to correctly reproduce the global stiffness of the structure. It is important to remark that the condition of 0 vertical displacement correspond to the position of the markers when the fuselage barrel touches the ground.

Concerning the frontal vertical displacements, the two experimental curves (Fig. 12-A) show a similar trend demonstrating that the mechanical response of the fuselage is almost unaffected by the roll angle measured during the drop test. Actually, the very small differences between these two experimental curves are comparable to the differences between the two numerical curves and can be attributed to the damage onset and evolution during the impact event which causes asymmetry in maximum displacements and maximum displacements times. Actually, a small difference can be appreciated between the mean numerical (420 mm) and the mean experimental (450 mm) maximum vertical displacement.

The comparison between the numerical and experimental lateral vertical displacements is introduced in Fig. 12-B. Actually, in this Figure, the displacement trends for the markers identified with B1 and B2 (see Fig. 6) for the experimental test and for the numerical model are reported.

As shown in the Fig. 12-B, the effect of the pitch angle produces a substantial difference in the trends of the two experimental curves. This variation between the front and the rear vertical displacements trends is also highlighted by the numerical curves. Hence, the comparison between the numerical and experimental lateral vertical displacements curves demonstrates that the effect of the pitch angle is not

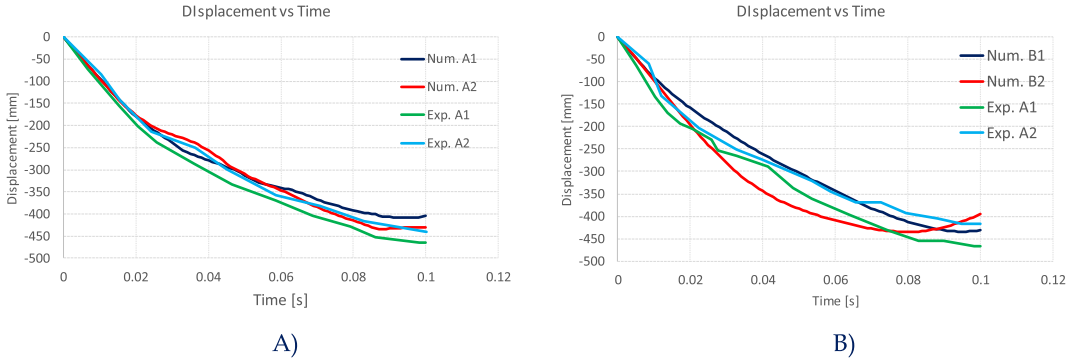

Fig. 12. Experimental and numerical Displacement vs time. A) Frontal displacements. B) Lateral displacements.

negligible and can be taken into account by the introduced numerical model. As consequence, an anticipation of the B1 curve with respect of B2 curve can be appreciated with shifted maximum vertical displacements. For the lateral vertical displacements markers B1 and B2, the mean numerical and the mean experimental maximum vertical displacement are almost identical (450 mm).

A further numerical-experimental comparison has been carried out between accelerations evaluated at the three different locations shown in Fig. 11. Fig. 13 shows the trends of the vertical accelerations as a function of time at the three analysed locations. Since the start and the duration of the experimental and numerical drop tests are not the same, the numerical curves have been shifted in time to be overlapped and compared to the experimental ones. Fig. 13-A introduces the acceleration trend for the accelerometer I (according to Fig. 11). Numerical and experimental curves show a similar trend even if the numerical model slightly underestimates the maximum acceleration peak. Only the maximum acceleration peak can be considered for numerical-experimental comparisons since the rest of the curve, due to the lack of the gravitational field in the numerical model, is not representative of the real mechanical response of the fuselage barrel subjected to the drop test. In Fig. 13-A, the experimental and the numerical trends of accelerations, for the accelerometer II located at the centre of the passenger's floor, are compared. Again, the figure shows a comparable trend between the experimental data and the values obtained from the numerical simulation with slight overestimation of the maximum peak. This effect can be due to the overestimation of the local stiffness mostly related to the type of connections applied between the fuselage sub-components. Indeed, as previously mentioned, the huge number of connections between the sub-components, at accelerometer II location, have been reproduced by tie constraint between the various surfaces, neglecting the presence of the rivets holes clearance and deformations. In Fig. 13-C, the experimental and the numerical trends of accelerations, for the accelerometer III located at the top of the fuselage barrel section. Again, the figure shows a comparable trend between the experimental data and the values obtained from the numerical simulation with a small overestima-

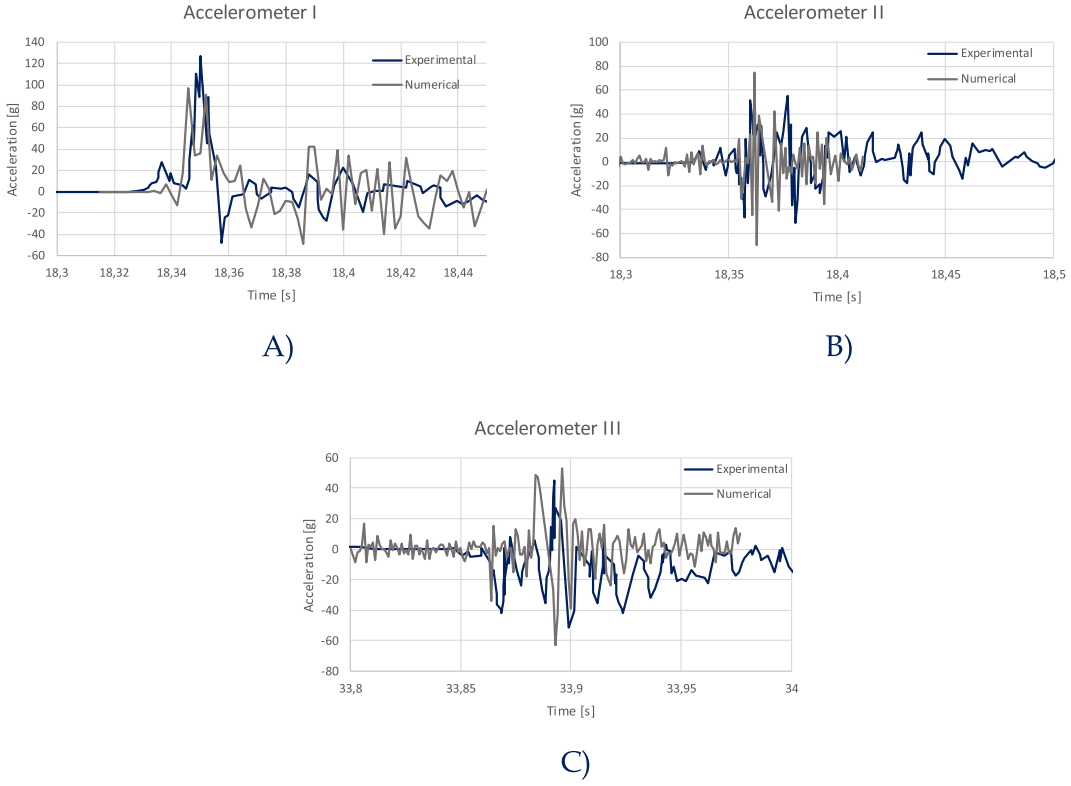

Fig. 13. Accelerometer versus time: A) Accelerometer I. B) Accelerometer II. C) Accelerometer III.

tion of the maximum and minimum peaks. Same considerations as for the accelerometer II apply. However, a slight oscillation in the numerical results for accelerometers II and III could be highlighted. This effect could be, probably, due to the propagation of the elastic waves between the barrel and the ground close to the impact location. This effect seems to not affect accelerometer I readings, probably because it is located very close to the impact location.

In order to better evaluate the capability of the proposed numerical model to mimic the global mechanical response of the fuselage barrel undergoing the drop test, in Fig. 14, a comparison between the global deformations of the test article and of the finite elements model at different time steps during the impact event, is introduced. Actually, in Fig. 14-A the onset of the impact event is represented (vertical displacement 0 mm and time 0 s; while, in Fig. 14-B an intermediate step

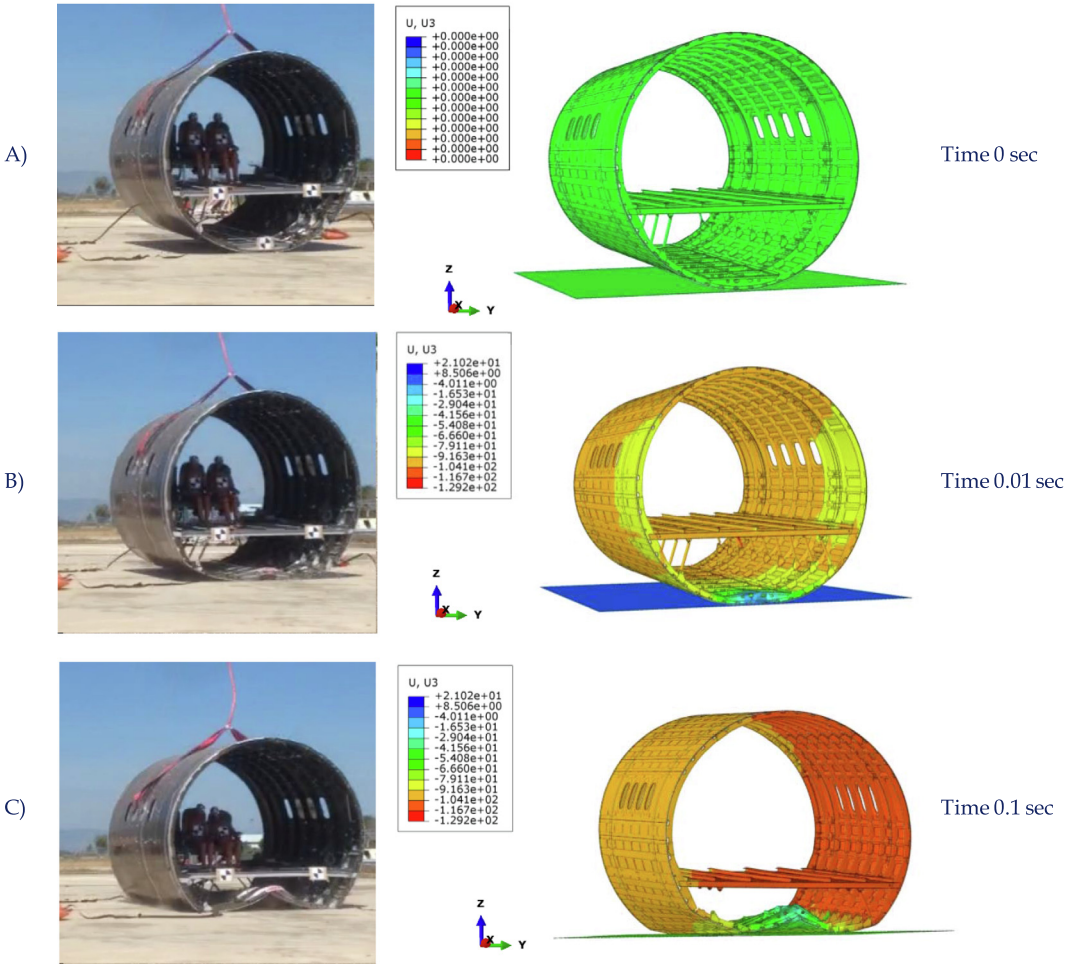

Fig. 14. experimental and numerical deformation comparisons for three different drop times. A) Time impact 0 s. B) Time impact 0.01 s. D) Time impact 0.1 s.

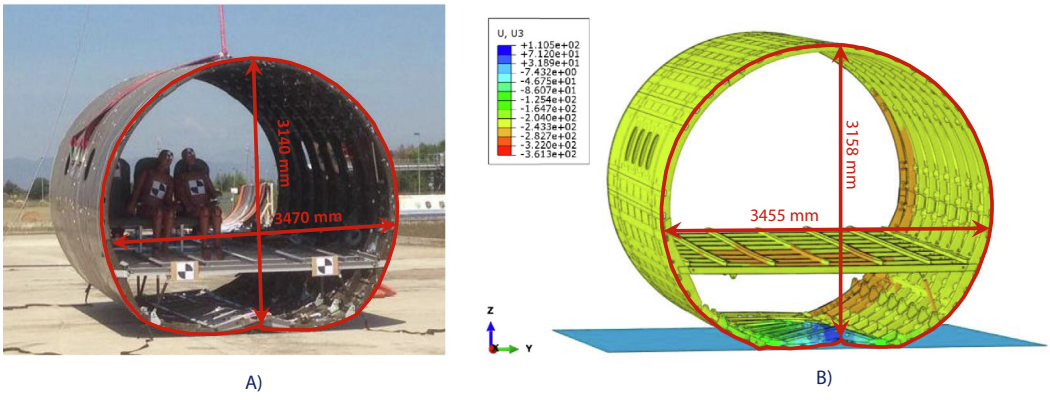

Fig. 15. Residual deformation after drop test. A) Experimental test article. B) Numerical model.

is represented (vertical displacement 100 mm and time 0,01 s). Finally, in Fig. 14- C the maximum vertical displacement step is represented (vertical displacement 430 mm and time 0,1 s). These comparisons, for all the considered time steps, show a general excellent agreement between the dropped fuselage barrel and the numerical model. The most of damages are located in the cargo area impacting with the ground in the front part of the fuselage. An extended frame failure between the passenger floor and the stanchion frame supports has been observed both experimentally and numerically.

In Fig. 15, the images of the test article at the end of the drop test (Fig. 15-A) and of the numerical model in the final stages of the ascent phase at maximum vertical displacement (Fig. 15-B), are compared. Although the final deformation of the numerical model is globally in good agreement with the test article deformation, quantitative differences in final (post impact) proportions can be observed. Actually, the numerical model results underestimate the residual deformations of the fuselage section, probably due to the lack of the rebound effect not introduced in the numerical simulation. To better appreciate the final deformation of the numerical model the vertical damaged stanchions had been removed from the Fig. 15-B.

The proposed numerical model has allowed to describe the evolution of the damage at lamina level for each sub-components during the drop test for the investigated fuselage barrel, differently from the experimental test which allow to provide the correct global behaviour of complex composite components without allowing to evaluate the history of the damage evolution locally. Hence the integration of experimental data and numerical results becomes of fundamental relevance to fully understand the failure mechanisms governing the energy absorption characteristics of the investigated fuselage barrel. The experimental evidences and the numerical outputs demonstrated that most critical sub-components involved in the drop test event able to govern the energy absorption characteristics of the investigated fuselage barrel are: the cargo area structure, the stanchions and the frames close to the cargo area.

The damage development and the failure status at the end of the drop tests are described in Fig. 16 and in Fig. 17. Fig. 16 introduces the damage development in the frames of the cargo area. Fig. 16-A presents an overview of the cargo area at the end of the drop test. The corresponding numerical output is provided in Fig. 16-B. The cargo area is the first component of the fuselage contributing to the absorption of the kinetic energy by fracture mechanisms. The failure of the frames in the cargo area starts in the front zone of the fuselage and propagates along the fuselage longitudinal direction. At the end of the drop test almost all the frames are broken in the middle of the section as shown in Fig. 16-C (image taken from experiments) and in Fig. 16-D (numerical output at the end of the analysis). A detail of the cargo area frames and floor support failure at the end of the drop test is introduced in Fig. 16-E (experimental) and Fig. 16-F (numerical). In the Fig. 17 A-B-C-D the numerically computed progression of damage in the frame support of the cargo area is introduced for different time steps (A: 0.005 sec B: 0.016 sec C: 0.022 sec E: 0.04 sec).

Fig. 18 presents the propagation of damage in terms of fibre failure in the frame and floor supports of the cargo area plotted on the undeformed structure for different time steps (A: 0.01 sec 5% damage of total cargo area; B: 0.02 sec 15% damage of total cargo area; C: 0.04 sec 25% damage of total cargo area; D: 0.07 sec 45% damage of total cargo area). The damage variable has been plotted on the cargo area frame and floor supports. Indeed, a value of the damage variable of zero (blue colour in Fig. 18) identifies a fully damaged element condition, while a value of one (red colour in Fig. 18) corresponds to no-

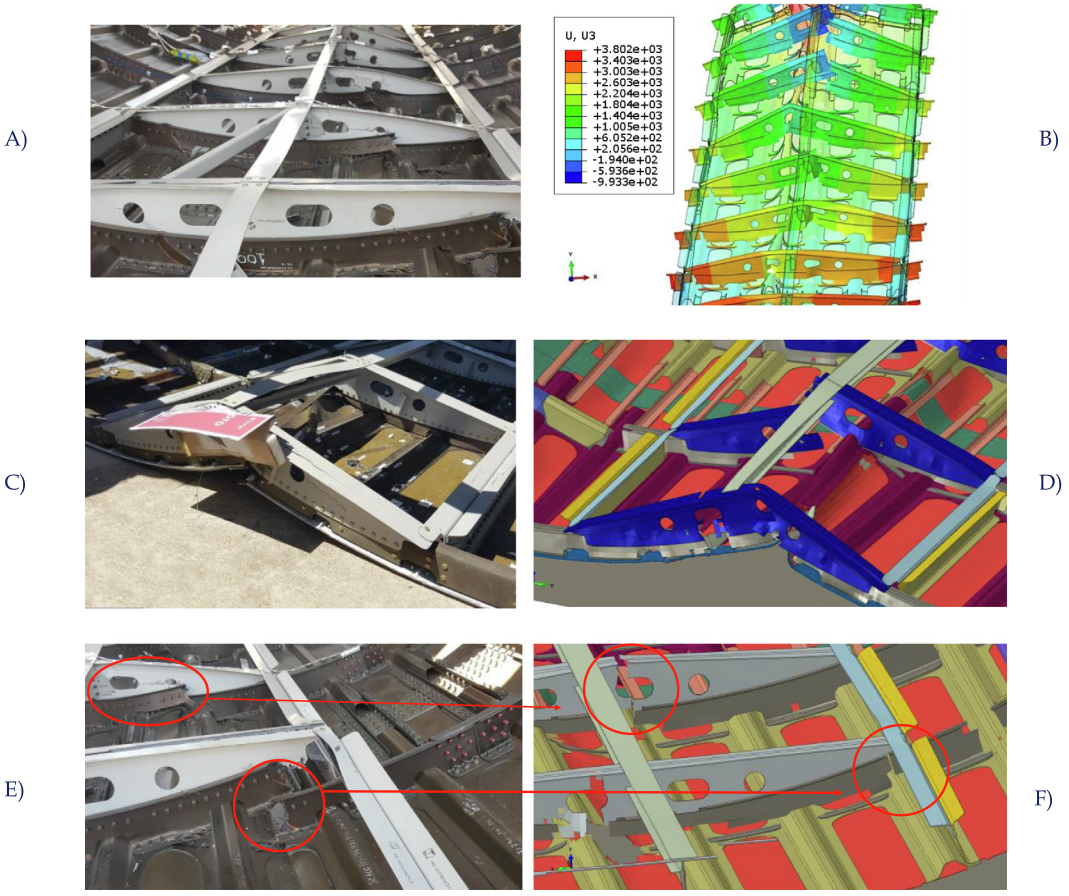

Fig. 16. Cargo Area Damages A-C-E) Experimental B-D-F) Maximum deformation numerical model.

damaged elements. Moreover, in Fig. 18, the other sub-components have been reported in translucency. The failure of the frames and floor supports in the cargo area starts in the front zone of the fuselage and propagates along the fuselage longitudinal direction. At the end of the drop test almost all the frames supports are broken as shown in Fig. 18-D.

As previously stated, the absorption of energy during the drop test of the investigated fuselage barrel has not been limited to the cargo area, but also to the stanchions connecting the floor to the frames. These connecting elements are expected to improve the passenger floor stiffness and reduce the accelerations transferred to the passenger cabin during a crash event. The breakage of stanchions actually strongly influences the acceleration peak transferred to the cabin and can cause asymmetry in the load distribution and in the damage evolution in the cargo area and in the passenger's floor. In Fig. 19 and in Fig. 20, the status at the end of the drop test and the damage evolution in the stanchions is illustrated, respectively. In Fig. 19- A, the broken stanchions at the end of the drop test are shown. At the end of drop test all the stanchions are broken except the last one in the rear part of the fuselage. This failure status is correctly predicted by the proposed numerical model as shown in Fig. 19-B.

Fig. 20 A-F allows to appreciate the evolution of the stanchions failure during the impact event at different time steps (A: 0.005 sec no Stanchions failure; B: 0.01 sec 2 Stanchions damaged; C: 0.014 sec 8 Stanchions damaged; D: 0.016 sec 10 Stanchions damaged; E: 0.022 sec 14 Stanchions damaged; F: 0.03 sec 18 Stanchions damaged;). Also

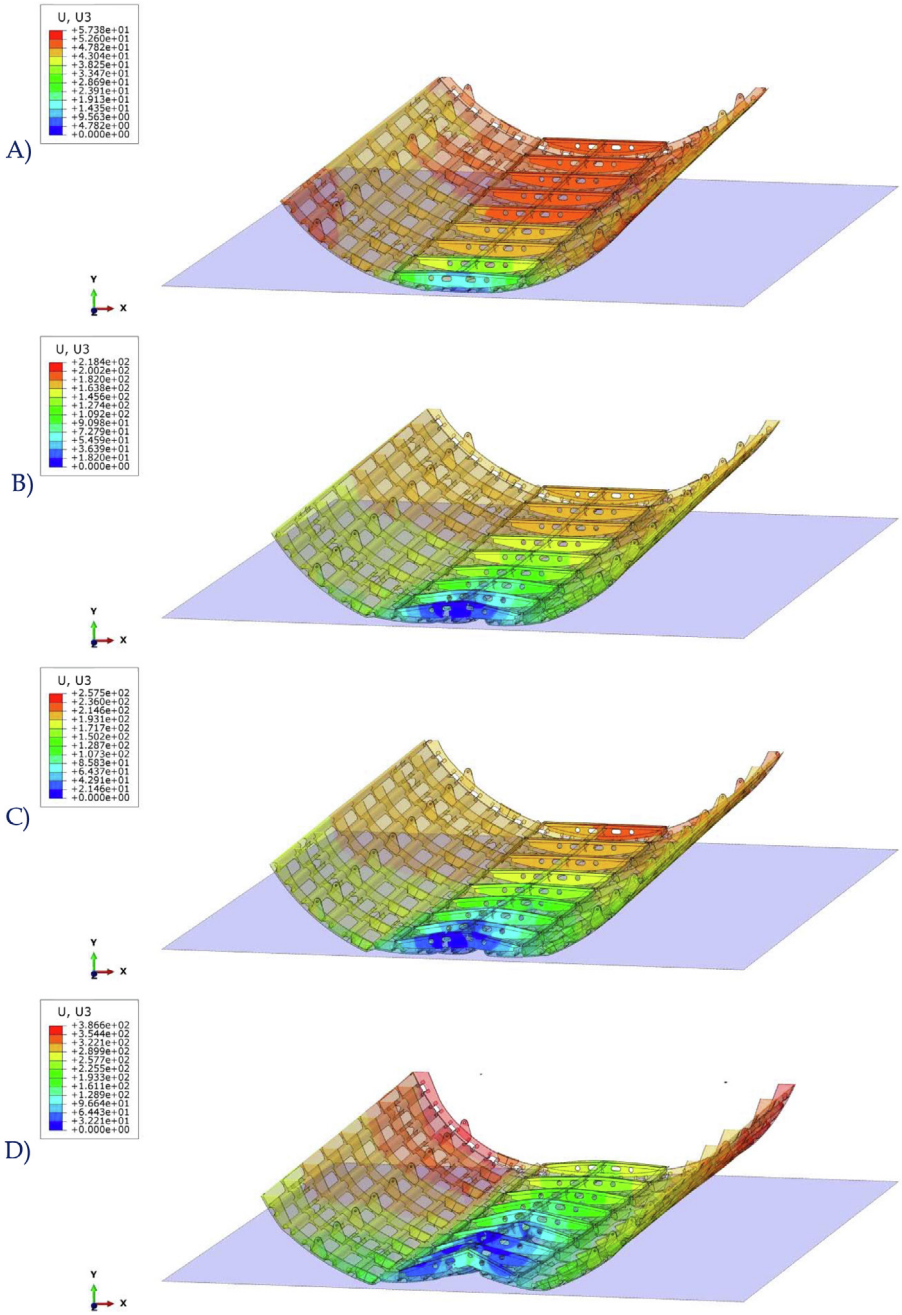

Fig. 17. (Impact direction along the negative value of z axis). Support Frame Damages numerical model. A: 0.005 sec B: 0.016 sec C: 0.022 sec E: 0.04 sec.

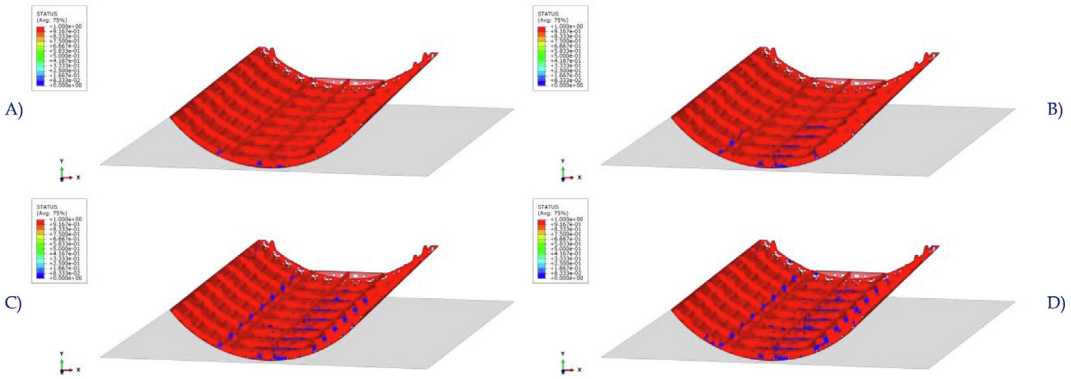

Fig. 18. Cargo Area (Impact direction along the negative value of z axis) Evolution of the fiber damage in the skin of the cargo area. A: 0.01 sec; B:0.02 sec; C:0.04 sec; D:0.07 sec.

in this case, as expected, the stanchions failure starts in the front part of the fuselage barrel and propagates to the rear area following the longitudinal direction. Elements (stanchions) which are no longer capable to absorb load have been removed in order to better appreciate the evolution of the damage in the fuselage barrel.

The final considerations on the absorption of energy during the drop test of the investigated fuselage barrel are related to the frames in the cargo area. These frames can be considered the most relevant structural component of the fuselage influencing the safety of occupants during a crash event. In Fig. 21 and in Fig. 22, the status at the end of the drop test and the damage evolution in the frames is illustrated, respectively. In Fig. 21- A-C, the broken frames at the end of the drop test are shown. At the end of drop test all the frames under the stanchions are broken, between the stanchion joints and the passenger floor joint. The last frame in the rear part of the fuselage shows a different damage location closed to the stanchion joint (this is probably the reason why the last stanchion does not fail). This final failure status is correctly predicted by the proposed numerical model as shown in Fig. 21-B-D.

Fig. 22 allows to appreciate the evolution of the frames failure during the impact event at different time steps (A: 0.002 sec; B: 0.004 sec; C: 0.005 sec; D: 0.007 sec). Also in this case, as expected, the frame failure starts in the front part of the fuselage barrel and propagates to the rear area following the longitudinal direction. The images in Fig. 22 represent the structure in the undeformed state, highlighting the undamaged elements in red colour and the fully damaged elements in blue colour

A Final overview of the fuselage barrel behaviour during the drop phase is given by the energy trends shown in Fig. 23. Fig. 23-A shows the energy absorbed by the system as elastic deformation. The difference between the total energy (at time step 0) and the energy recovered as elastic deformation energy represents the energy dissipated as fracture energy and plastic deformation energy. Fig. 23-B shows the energy dissipated as fracture energy. The fracture energy rate is about 30% of the kinetic energy at time t = 0.

5. Conclusions

In the present work, an experimental–numerical study on the crashworthiness of a composite fuselage barrel for civil aircraft transportation has been presented. Experimental data from a drop test have been used, together with numerical results from a proposed advanced numerical model, to investigate the damage onset and evolution influence on the global mechanical response of the fuselage barrel during the crash event. The Abaqus/Explicit finite elements environment has been chosen for the implementation of the proposed numerical model which uses Hashin's Failure Criteria and gradual material properties degradation rules to simulate, respectively, the intra-laminar damage onset and evolution in composite sub-components; while, for the aluminium alloy, a failure criterion for ductile metallic materials has been adopted. The preliminary comparisons, between experimental data and numerical results, in terms of vertical displacements, accelerations and global deformations of the structure, demonstrated the excellent capabilities of the proposed numerical

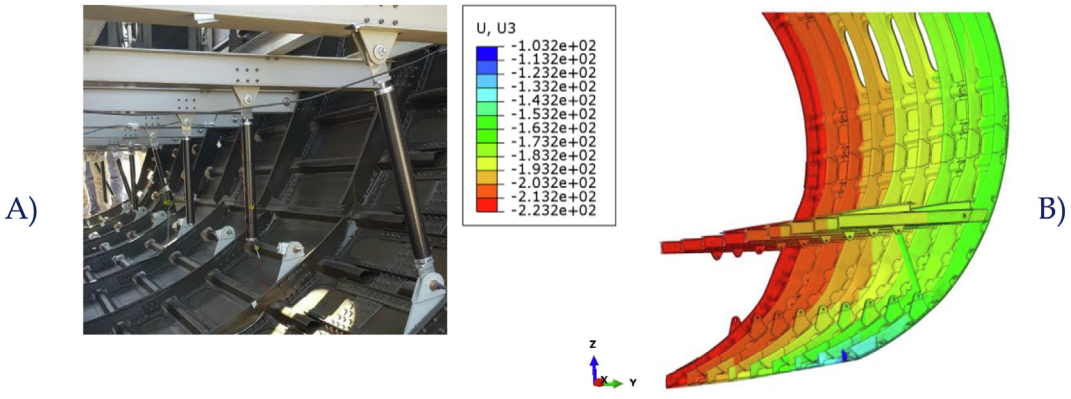

Fig. 19. Stanchions Failure at the end of the drop test A) Experimental image B) Numerical results.

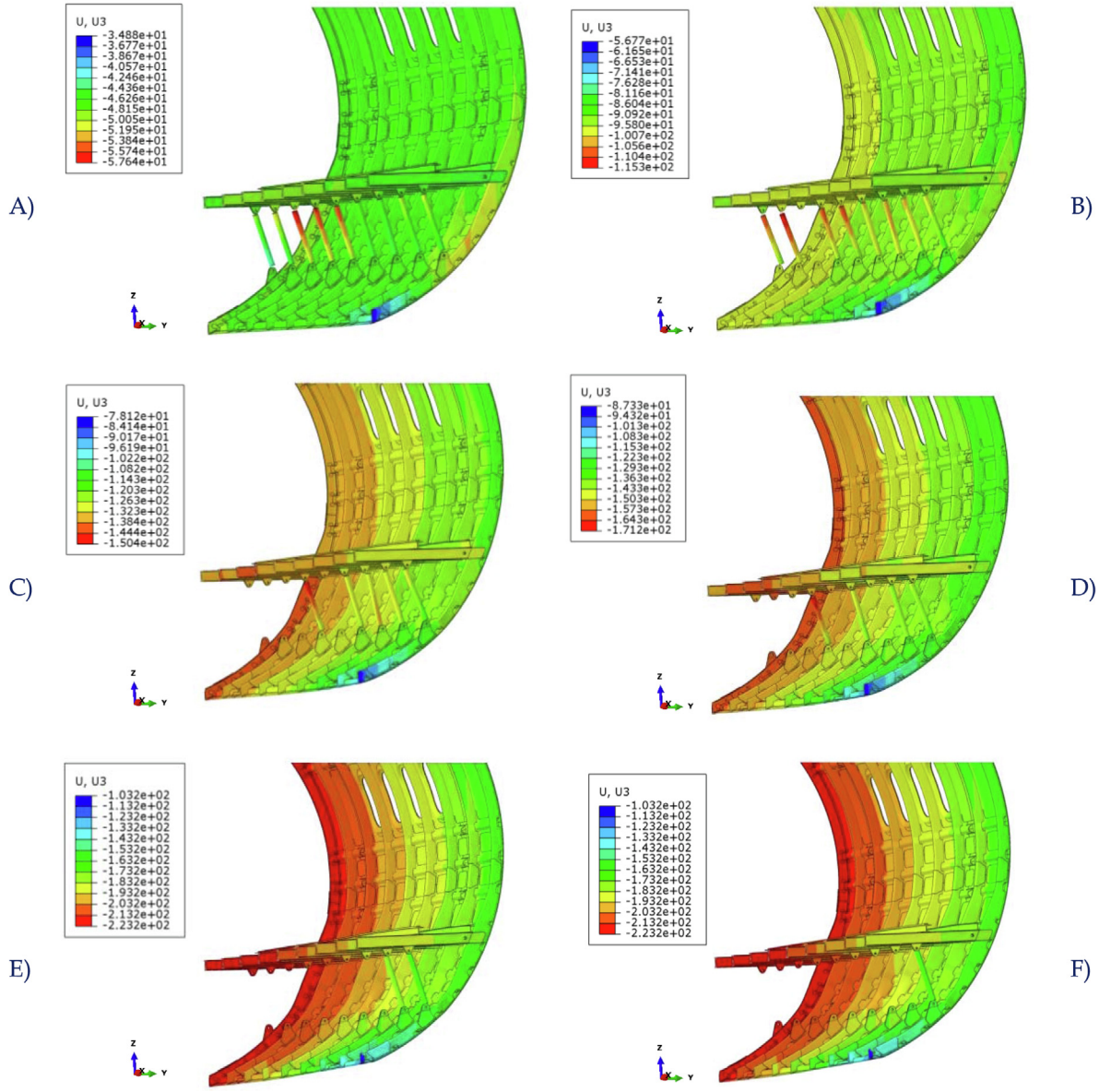

Fig. 20. Numerical damage progression in the Stanchions during the drop test. A: 0.005 sec; B:0.01 sec; C:0.014 sec; D:0.016 sec; E:0.022 sec; F:0.03 sec.

model to provide a realistic simulation of the drop test event and to consider the influence of drop test variables (ex. pitch angle) on the global structural deformations. The effects of the introduced modelling approximations, especially in terms of connections between sub-components, on the evaluation of the global stiffness prediction of the structure, have been also assessed and considered tolerable for the investigated test case. Following the drop test simulation, from a cross-comparison of experimental observations and final damage status of the model, the cargo area supporting structure, the stanchions and the cargo area frames have been identified as key sub-components influencing the kinetic energy absorption and, hence, the crashworthiness of the investigated fuselage barrel. Indeed, the cargo structure has been found to be the sub-component experience the most of the impact induced damage and which mostly influence the energy absorption capability of the fuselage. On the other hand, the stanchions and the cargo frames have been found to play an important role in accelerations to occupants transfer mitigation and in general in occupants' safety preservation. Actually, the numerically predicted damage evolution in these key sub-components has been assessed providing justifications of the experimentally observed final damage status at the end of the drop test. As expected, due to the pitch angle effect, the damage in the cargo area structure and in the stanchions has been found to on-set in the front area of the fuselage barrel and to propagate along the longitudinal direction toward the rear area, following a non-symmetrical trend. A more complex propagation has been found for the cargo area frames, whose failure is, however, somehow dependent on the stanchions' failure sequence. Finally, as a result of the integration, between the adopted advanced numerical model and the experimental observations, proposed in this paper, a substantial improvement of the understanding of the dynamic behaviour during the drop test, at sub-component (local) level, has been achieved. This improved understand of the local phenomena. which cannot be guaranteed by the experimental observation of a drop test of a very complex structure, is expected to provide indications towards a more reliable crashworthy design of aerospace composite components.

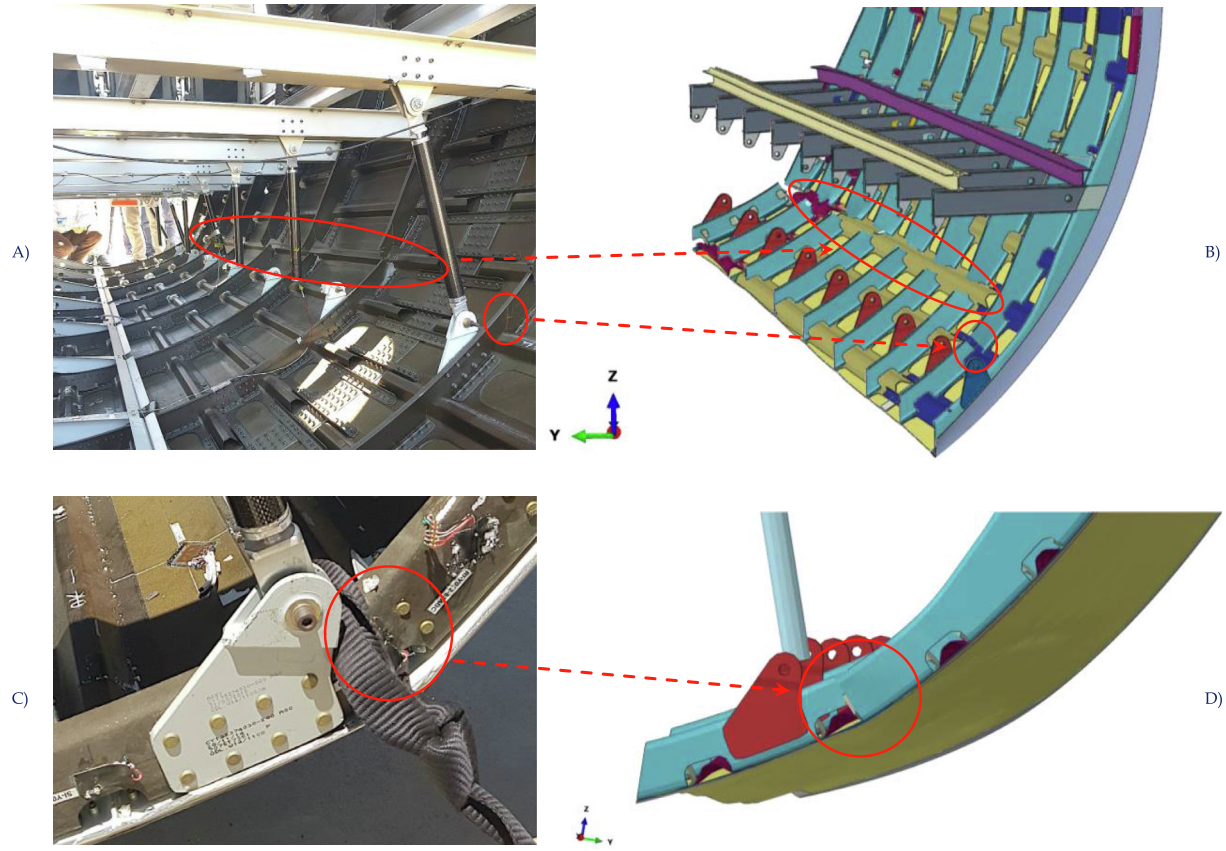

Fig. 21. Frame Failure at the end of the drop test A) Experimental image rear right view. B) Numerical result rear right view. C) Experimental image frontal right view. D) Numerical result frontal right view.

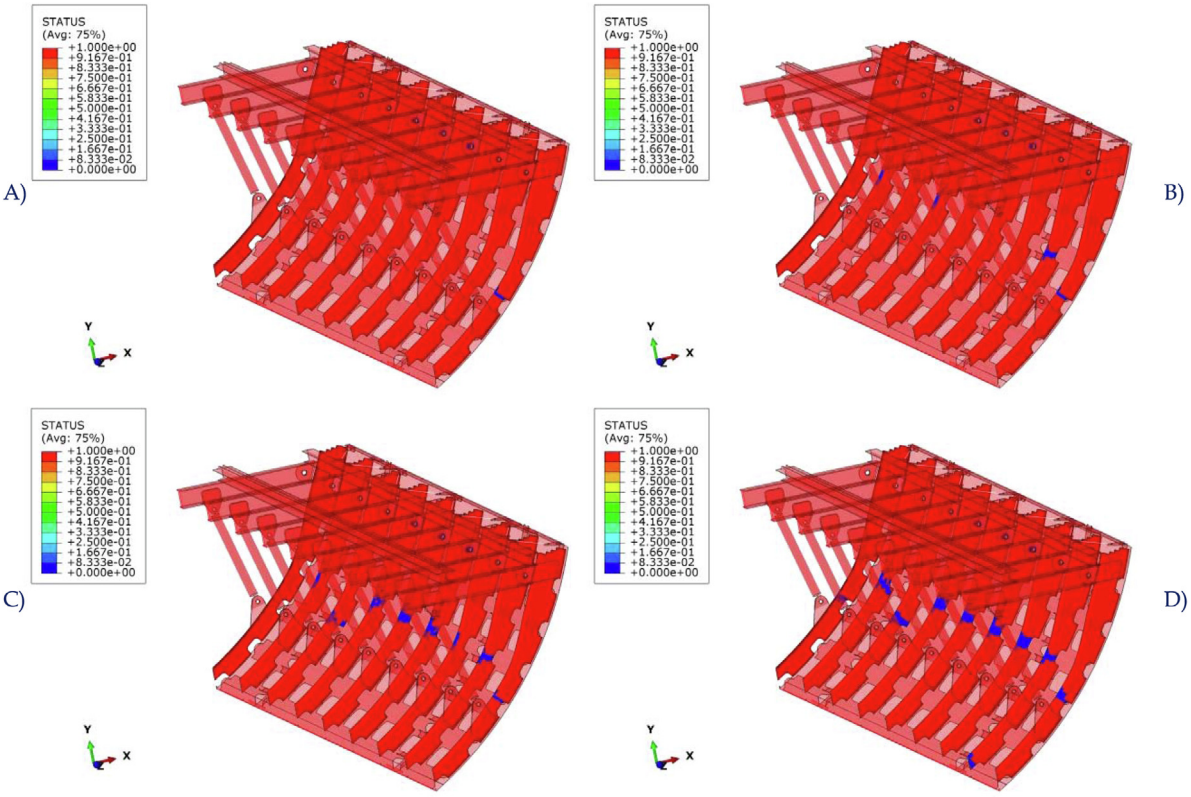

Fig. 22. Numerically computed frame failure progression during the drop test. A: 0.002 sec; B:0.004 sec; C:0.005 sec; D:0.007 sec.

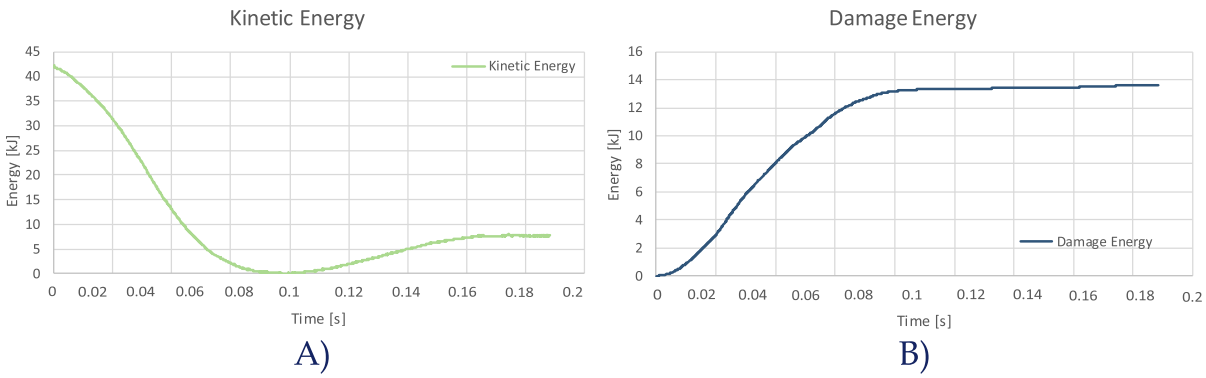

Fig. 23. Energies vs time, A:Kinetic energy. B: Damage energy.

CRediT authorship contribution statement

A. Riccio: Conceptualization, Methodology, Formal analysis, Investigation, Writing - original draft. **S. Saputo:** Conceptualization, Methodology, Formal analysis, Investigation, Writing - original draft. **A. Sellitto:** Conceptualization, Methodology, Formal analysis, Investigation, Writing - original draft. **F. Di Caprio:** Conceptualization, Methodology, Formal analysis, Investigation, Writing - original draft. **L. Di Palma:** Conceptualization, Methodology, Formal analysis, Investigation, Writing - original draft.

Declaration of Competing Interest

The authors declare that they have no known competing financial interests or personal relationships that could have appeared to influence the work reported in this paper.

Acknowledgments

The Research presented in this paper is part of follow-on activities of the project CERVIA (Innovative and Advanced Verification and CERtification methods) funded by Italian Minister Research Program Programma Operativo Nazionale 2007–2013 through the Programma Operativo Regionale–Fondo Europeo SviluppoRegionalefundsmanaged by RegioneCampania, promoter Distretto Aerospaziale della Campania (DAC). Authors would like to thank the CIRA personnel for the precious support for the experimental data recovery and analysis.

References

[1] Yu Z, Zhou X, Zhou X, Zhang Y, Zhu Q. Crashworthy subfloor structure of civil aircraft via inclined inward-folding composite tubes. Compos B Eng 2020;189:107887. https://doi.org/10.1016/j.compositesb.2020.107887.
[2] Zhang Z, Sun W, Zhao Y, Hou S. Crashworthiness of different composite tubes by experiments and simulations. Compos B Eng 2018;143:86–95.
[3] McCarthy MA, Wiggenraad JFM. Numerical investigation of a crash test of a composite helicopter subfloor structure. Compos Struct 2001;51(4):345–59.
[4] Laban Othman, Gowid Samer, Mahdi Elsadig, Musharavati Farayi. Experimental investigation and artificial intelligence-based modeling of the residual impact damage effect on the crashworthiness of braided Carbon/Kevlar tubes. Compos Struct 2020;243:112247. https://doi.org/10.1016/j.compstruct.2020.112247.
[5] Habibi M, Selmi S, Laperrière L, Mahi H, Kelouwani S. Experimental investigation on the response of unidirectional flax fiber composites to low-velocity impact with after-impact tensile and compressive strength measurement. Compos B Eng 2019;171:246–53.
[6] Nikbakht M, Yousefi J, Hosseini-Toudeshky H, Minak G. Delamination evaluation of composite laminates with different interface fiber orientations using acoustic emission features and micro visualization. Compos B Eng 2017;113:185–96.
[7] Fu Chen, Wang Xi. Micro-mechanical analysis of matrix crack-induced delamination in cross-ply laminates in tension. Compos Struct 2020;243:112202. https://doi.org/10.1016/j.compstruct.2020.112202.
[8] Sellitto A, Borrelli R, Caputo F, Riccio A, Scaramuzzino F. Application of the mesh superposition technique to the study of delaminations in composites thin plates. Key Eng Mater 2012;525–526:533–6.
[9] Kindervater Ch. Validation of crashworthiness simulation and design methods by testing of a scaled composite helicopter frame section. AHS conference, May; 2011.
[10] Jackson A, Dutton S, Gunnion AJ, Kelly DW. Effect of manufacture and laminate design on energy absorption of open carbon-fibre/epoxy sections. In: 17th Int Conf Compos Mater (ICCM-17). Edinburgh, UK; 2009.
[11] Lo Cascio M, Milazzo A, Benedetti I. Virtual element method for computational homogenization of composite and heterogeneous materials. Compos Struct January 2020;232:15.
[12] Gulizzi Vincenzo, Benedetti Ivano, Milazzo Alberto. A novel boundary element formulation for anisotropic fracture mechanics. Theor Appl Fract Mech 2019;104:102329. https://doi.org/10.1016/j.tafmec.2019.102329.
[13] Cronkhite JD, Berry VL. Crashworthy airframe design concepts fabrication and testing, NASA Contractor Report no. 3603, NASA, Washington, DC; 1982.
[14] Fasanella EL, Widmayer E, Robinson MP. Structural analysis of the controlled impact demonstration of a jet transport airplane. J Aircraft 1987;24:274–80.
[15] Flight Safety Foundation, Army aviation safety with reference to crash injury and crashworthiness programs, TREC Tech. Rep., Flight Safety Foundation, Alexandria, VA, 30 December 1960.
[16] Adams A, Lankarani HM. A modern aerospace modelling approach for evaluation of aircraft fuselage crashworthiness. Int J Crashworthiness 2003;8:401–13.
[17] Wiggenraad JFM, Michielsen ALPJ, Santoro D. Finite element methodologies development to simulate the behaviour of composite fuselage structure and correlation with drop test. Air Space Europe 2001;3:228–1223.
[18] Jackson KE, Fasanella EL. Development of a scale model composite fuselage concept for improved crashworthiness. J Aircraft 2001;38:95–103.
[19] Meng FX, Zhou Q, Yang JL. Improvement of crashworthiness behaviour for simplified structural models of aircraft fuselage. Int J Crashworthiness 2009;14:83–97.
[20] Ren Y, Xiang J. A comparative study of the crashworthiness of civil aircraft with different strut configurations. Int J Crashworthiness 2010;15:311–30.
[21] Zheng J, Xiang J, Luo Z. Crashworthiness layout of civil aircraft using waved-plate for energy absorption. Acta Aeronaut Astronaut Sin 2010;32:1396–402.
[22] Kumakura I, Minegishi M, Iwasaki K. Impact simulation of simplified structural models of aircraft fuselage, SAE Tech. Paper 2000-01-5586, 2000.
[23] Ren Y, Xiang J. The crashworthiness of civil aircraft using different quadrangular tubes as cabin-floor struts. Int J Crashworthiness 2011;16:253–62.
[24] Shoji H, Miyaki H, Iwasaki K, Minegishi M. Crashworthiness research on cabin structure at JAXA, 5th Triennial International Aircraft Fire and Cabin Safety Research Conference, Atlantic City, NJ; 2007.
[25] Zhang XW, Yang JL, Yu TX. Elastic-plastic behavior of a semicircular frame being pressed against a rigid plane. Acta Mech Sin 2008;24:419–31.
[26] Pérez José G. Energy absorption and progressive failure response of composite fuselage frames. Master thesis. Juli: Virginia Polytechnic Institute; 1999.
[27] Hashemi R. Sub-component dynamic tests on an A310 rear fuselage, Cranfield Impact Centre Limted, Sub-task 2.4 of the European Community funded research project 'Crashworthiness for commercial aircraft; 1994.
[28] Waimer M. The kinematics model – a numerical method for the development of a crashworthy composite fuselage design of transport aircraft. In: Sixth triennial international aircraft fire and cabin safety research conference, October; 2010.
[29] Subbaramaiah R, Prusty BG, Pearce GMK, Lim SH, Thomson RS. Crashworthy response of fibre metal laminate top hat structures. Compos Struct 2017;160:773–81.
[30] Izzi MI, Montemurro M, Catapano A, Jérôme Pailhès J. A multi-scale two-level optimisation strategy integrating a global/local modelling approach for composite structures. Compos Struct 2020;237.
[31] Waimer M. Development of a kinematics model for assessment of global crash scenarios of a composite transport aircraft fuselage PhD thesis. University of Stuttgart; 2013.
[32] Ren Y, Xiang J. Energy absorption structures design of civil aircraft to improve crashworthiness. Aeronaut J 2014;118:383–98.
[33] Santiago RC, Cantwell WJ, Jones N, Alves M. The modelling of impact loading on thermoplastic fibre-metal laminates. Compos Struct 2018;189:228–38.

[34] Sturm R, Klett Y, Kindervater Ch, Voggenreiter H. Failure of CFRP airframe sandwich panels under crash-relevant loading conditions. Compos Struct 112, 2014.
[35] Di Benedetto RM, Botelho EC, Gomes GF, Junqueira DM, Ancelotti Junior AC. Impact energy absorption capability of thermoplastic commingled composites. Compos B Eng 2019;176.
[36] Zheng J, Xiang J, Luo Z, Ren Y. Crashworthiness design of transport aircraft subfloor using polymer foams. Int J Crashworthiness 2011;16:375–83.
[37] Wu QG, Wen HM, Qin Y, Xin SH. Perforation of FRP laminates under impact by flat-nosed projectiles. Compos B Eng 2012;43(2):221–7. https://doi.org/10.1016/j.compositesb.2011.08.045.
[38] Fatt MSH, Lin C. Perforation of clamped, woven E-glass/polyester panels. Compos B Eng 2004;35(5):359–78.
[39] XiaochuanL, JunG, ChunyuB, XiashengS, RangkeM. Drop test and crash simulation of a civil airplane fuselage section. Chin J Aeronaut 2015;28(2):447–56.
[40] Kuraishi A, Tsai SW, Liu KKS. A progressive quadratic failure criterion, Part B. Compos Sci Technol 2002;62(12):1683–95.
[41] Spahn J, Andrä H, Kabel M, et al. A multiscale approach for modeling progressive damage of composite materials using fast Fourier transforms. Comput Meth Appl Mech Eng 2014;268:871–83.
[42] Pineda EJ, Waas AM, Bednarcyk BA, et al. Progressive damage and failure modeling in notched laminated fiber reinforced composites. Int J Fract 2009;158(2):125–43.
[43] Basu S, Waas AM, Ambur DR. Prediction of progressive failure in multidirectional composite laminated panels. Int J Solids Struct 2007;44(9):2648–76.
[44] Apalak ZG, Apalak MK, Genc MS. Progressive damage modeling of an adhesively bonded unidirectional composite single-lap joint in tension at the mesoscale level. J Thermoplast Compos Mater 2006;19(6):671–702.
[45] Ridha M, Wang CH, Chen BY, et al. Modelling complex progressive failure in notched composite laminates with varying sizes and stacking sequences. Compos A Appl Sci Manuf 2014;58:16–23.
[46] Pineda EJ, Waas AM. Modelling progressive failure of fibre reinforced laminated composites: mesh objective calculations. Aeronaut J 2012;116(1186):1221–46.
[47] Riccio A, Cristiano R, Saputo S, Sellitto A. Numerical methodologies for simulating bird-strike on composite wings. Compos Struct 2018;202:590–602.
[48] Nagle Anthony, Wowk Diane, Marsden Catharine. Three-dimensional modelling of interlaminar normal stresses in curved laminate components. Compos Struct 2020;242:112165. https://doi.org/10.1016/j.compstruct.2020.112165.
[49] Di Palma L, Di Caprio F, Chiariello A, Ignarra M, Russo S, Riccio A, De Luca A, Caputo F. Vertical drop test of composite fuselage section of a regional aircraft. AIAA J 2020;58(1):474–87. https://doi.org/10.2514/1.J058517.
[50] Hashin Z. Failure criteria for unidirectional fiber composites. J Appl Mech 1980;47:329–34.
[51] Sellitto A, Borrelli R, Caputo F, Riccio A, Scaramuzzino F. Application to plate components of a kinematic global-local approach for non-matching finite element meshes. Int J Struct Integrity 2012;3(3):260–73.
[52] Hooputra H, Gese H, Dell H, Werner H. A comprehensive failure model for crashworthiness simulation of aluminium extrusions. Int J Crashworthiness 2004;9(5):449–64.